ACS APPLIED MATERIALS & INTERFACES

www.acsami.org Research Article

Triplet Energy Transfer from Lead Halide Perovskite for Highly Selective Photocatalytic 2 + 2 Cycloaddition

Yixiong Lin, Mariana Avvacumova, Ruilin Zhao, Xihan Chen, Matthew C. Beard, and Yong Yan*

Cite This: https://doi.org/10.1021/acsami.2c03411 Read Online

ACCESS | Metrics & More | Article Recommendations | Supporting Information

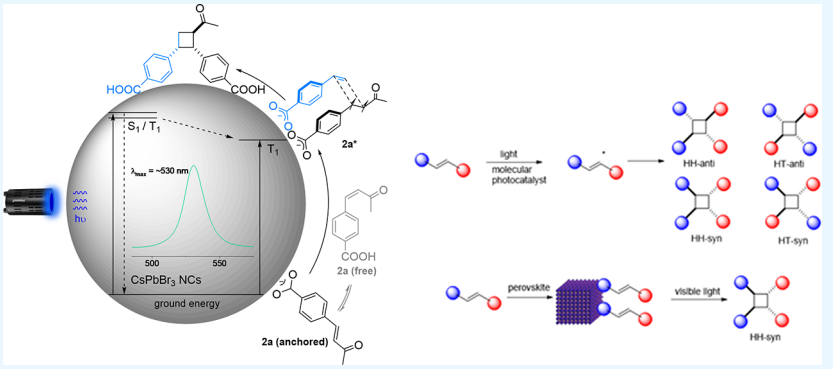

ABSTRACT: Triplet excitons are generally confined within a semiconductor. Hence, solar energy utilization via direct triplet energy transfer (TET) from semiconductors is challenging. TET from lead halide perovskite semiconductors to nearby organic molecules has been illustrated with ultrafast spectroscopy. Direct utilization of solar energy, *i.e.*, visible light, via TET for photocatalysis is an important route but has not yet been demonstrated with lead halide perovskite semiconductors. Here, we show that a photocatalytic reaction, focusing on a 2 + 2 cycloaddition reaction, can been successfully demonstrated via TET from lead halide perovskite nanocrystals (PNCs). The triplet excitons are shown to induce a highly diastereomeric *syn*-selective 2 + 2 cycloaddition starting from olefins. Such photocatalytic reactions probe the TET process previously only observed spectroscopically. Moreover, our observation demonstrates that bulk-like PNCs (size, >10 nm; PL = 530 nm), in addition to quantum-confined smaller PNCs, are also effective for TET. Our findings may render a new energy conversion pathway to employ PNCs via direct TET for photocatalytic organic synthesis.

KEYWORDS: *triplet energy transfer, perovskite, 2 + 2 cycloadditions, photocatalysis, semiconductor nanocrystals*

1. INTRODUCTION

Lead halide perovskite semiconductors have been discovered as highly efficient systems for photovoltaics, photodiodes, sensitive photodetectors, etc.,[1] due to their unique optoelectronic properties, particularly high energy absorption efficiency,[2] light-induced long-lived charge carriers,[3,4] long carrier diffusion lengths, etc.[5,6] We[7−9] and others[10−14] have exploited such outstanding photophysical behavior of metal halide perovskite nanocrystals (PNCs) for use in photoredox organic synthesis reactions. The principle that we strive to exploit is that of the long-lived charge-separated state and subsequent high charge transfer efficiency to activate organic substrates so as to gain or lose electrons for the key step necessary in redox-based organic reaction catalytic cycles. The power energy conversion efficiency of lead halide perovskite solar cells has reached 25% within a decade of development, implying that the energy transformation (*i.e.*, solar to electric energy) process is an efficient process in these semiconductors.[15] Utilization of visible light, a major portion of solar energy, captured via long-lived triplet states has been widely applied with particular interest in photocatalytic organic synthesis.[16−21]

Direct utilization of long-lived triplet states using molecular chromophores for organic activation has been extensively explored.[16−21] However, employment of triplet excitons from inorganic semiconductors is usually challenging, because such excitons are generally tightly confined within the semiconductor. Notable exceptions have been recently reported, *e.g.*, pioneering work of the direct observation of triplet energy transfer (TET) from CdSe quantum dots (QDs) to organic molecules[22] and triplet exciton transfer from CdSe QDs for organic substrate activation and subsequent regio- and

Received: February 23, 2022
Accepted: May 11, 2022

diastereoselective or chemo- and stereoselective cycloadditions that cannot be otherwise achieved by molecular photocatalysts.[23,24] Lately, TET from PNCs to the triple state of suitable organic molecules (*e.g.*, polycyclic aromatic hydrocarbons, PAHs,[25,26] and rhodamine B[27]) has been explored via ultrafast spectroscopy. Note that a detailed mechanistic study revealing a singlet-energy-transfer mechanism from lead halide perovskite to rhodamine B is also reported.[28] Overall, such energy transfer processes are mainly observed via the organic triplet energy acceptor that further induces triplet−triplet annihilation upconversion (TTA-UC). Notably, an early report of triplet sensitization of PNCs for such TTA-UC application can be traced back to 2017, where Mase *et al.* employed lead halide PNCs to excite the triplet of the surface-bound organic dye molecules. They achieved an efficient upconversion via a subsequent TET to 9,10-diphenylanthracene (DPA).[29] Direct application of such an energy transfer process in organic substrate activation via lead halide PNCs, *i.e.*, photocatalysis,[27,30] has been predicted; however, it has not yet been experimentally achieved.

Here, we report the first lead halide perovskite-based TET process employed in a photocatalytic organic system, and we found that PNCs (bulk-like, larger than the Bohr radius; size, >10 nm; E_{CB} = −1.2 V, E_{VB} = 1.2 V, all vs SCE, CB = conduction band, VB = valence band;[31] triplet energy, E_G = 2.4 eV) can induce diastereomeric *syn*-selective 2 + 2 olefin cycloadditions. Lately, visible light-induced TET-mediated intermolecular 2 + 2 cycloaddition has been reported by Yoon *et al.*,[17,32] Bach and Alonso,[33] Wu *et al.*,[16] and others,[34,35] where an organic chromophore or Ir, Ru-based transition metal photocatalysts were utilized. Therefore, the light-induced intermolecular 2 + 2 cycloaddition was chosen here as a model reaction to probe the TET ability of the PNCs (Figure 1). TET from the long-lived triplet states of a molecular photocatalyst usually leads to a free (unbound) substrate triplet state, which may result in nonselective 2 + 2 couplings, as shown in Scheme 1. Our approach here utilizes the PNC surfaces as a template via the dynamic anchoring of the organic substrates. Such anchoring encourages efficient TET from the

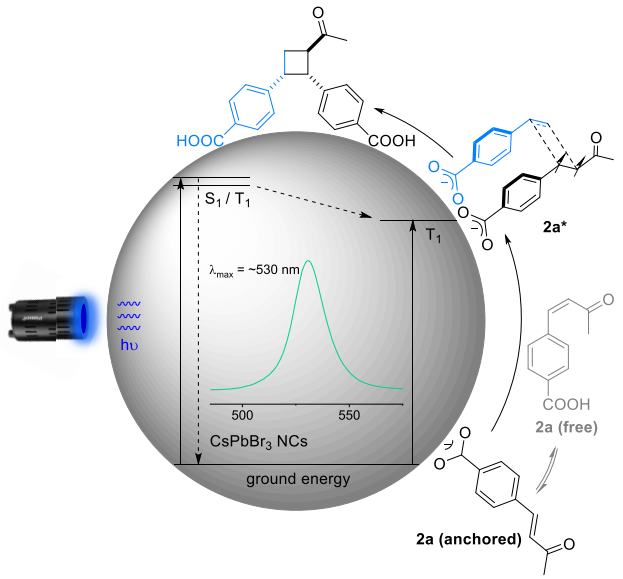

Figure 1. Proposed mechanism of visible light-induced $CsPbBr_3$ NC TET-mediated precise intermolecular 2 + 2 cycloaddition.

Scheme 1. TET-Based 2 + 2 Cycloadditions[a]

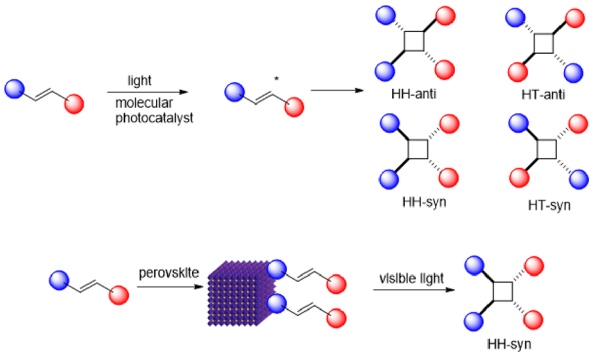

[a]Molecule- and perovskite-induced photocatalysis. HH: head-to-head; HT: head-to-tail.

PNCs to the surface-bound substrates, followed by the 2 + 2 cycloaddition on the PNC surface, hence leading to a regioselective head-to-head (HH-) 2 + 2 product. Moreover, a surface *syn*-binding mode rather than *anti*-mode can be encouraged, yielding a highly selective 2 + 2 *syn*-cyclobutane product. Note that a charge transfer-induced stereoselective C−C coupling reaction via perovskite QDs was reported lately,[36] although the selectivity remains governed by a thermodynamic driving force similar to previous work.[37] Here, our TET approach induces a unique thermodynamically unfavored 2 + 2 *syn*-selective cycloaddition that cannot be achieved by homogeneous molecular photocatalysts.

In addition, bulk-like PNC-induced 2 + 2 cycloaddition of olefins may also demonstrate a noticeable discrepancy to a previous TET photocatalytic approach using quantum-confined CdSe.[23] While quantum-confined semiconductors have been constantly employed to demonstrate feasible interfacial TET from inorganic QDs to organic molecules,[38−40] TET from bulk perovskite has only been lately illustrated in a solid-state upconversion device.[41] Bulk perovskite film-based TET, which substantially circumvents poor exciton diffusion in previous QD-sensitized devices, can be precisely achieved by controlling interfacial properties of fully solution-processed devices.[41] Bulk-like materials that may be easily accessible and produced in substantially larger quantities[7,42] render unique properties of the perovskite NCs used here over other quantum-confined systems for photocatalytic reactions, offering an appealing route to possible future industrial scaleup.

2. RESULTS AND DISCUSSION

2.1. Triple Energy Acceptor (TEA). TEA plays a vital role in the NC-based TET process. Spectroscopically, Wu *et al.* reported that strong quantum confinement is imperative for efficient TET from the PNCs to carboxylate-linked PAH acceptors.[25,27] Castellano *et al.* used polyaromatic carboxylic acid as a TET acceptor to directly observe TET from CdSe semiconductor NCs via transient absorption spectroscopy[22] and to study the delayed molecular triplet generation from PbS QDs.[43] Tang *et al.* used a series of anthracene carboxylic acid derivatives with variable bridging length to study the distance-dependent TET of CdSe NCs,[44] and the carboxylic acid-bearing transmitters were also discussed.[45] Weiss *et al.* demonstrated TET to vinylbenzoic acid derivatives from CdSe QDs.[23,24]

Here, we screen the olefin substrates to probe the TET process from PNCs. We first explore TET to olefin substrates

https://doi.org/10.1021/acsami.2c03411
ACS Appl. Mater. Interfaces XXXX, XXX, XXX−XXX

via Stern–Volmer quenching studies as shown in Figure 2. Meaningful PL quenching as indicated by the quenching

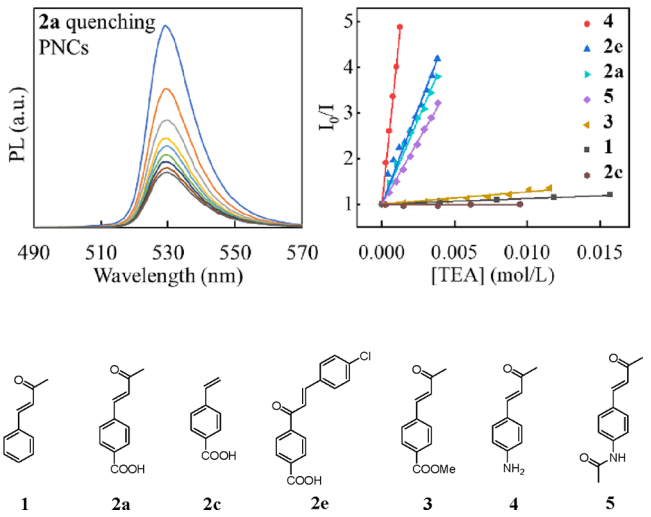

Figure 2. Stern–Volmer quenching studies of various olefin TEAs with PNCs.

constant, K_{SV}, was only observed on the TEAs with amine- or carboxylate-anchoring groups, such as **2a**, **2e**, and **4**. Negligible quenching was shown when such anchoring was missing in **1** or diminishing upon esterification of the acid in **3**. Compound **2c** also illustrated no TET, probably because the energy of the triple state, E_T, of styrene (~2.51 eV[23]) is higher than that of the bulk-like PNCs triplet state (2.4 eV). Overall, suitable olefin TEAs for bulk PNCs are generally substrates with lower E_T and with a suitable carboxylic acid- or amine-anchoring group. It is important to note here that we cannot distinguish the quenching process of amine-anchoring **4** via TET or charge transfer process as previously described,[27,42] even though the highest quenching constant was observed. **5** also demonstrates significant quenching even after acetylation of the amine group that may diminish the amine's binding ability to the PNCs. However, cycloaddition of **4** and **5** is not successful, likely because VB-based amine oxidation (charge transfer process) is dominant, as previously observed using PNCs.[27,42]

2.2. Surface Binding. Surface binding is imperative for surface-template photocatalytic reactions. TEA's dynamic binding to the PNC surface is explored using NMR. The binding of the substrate, *i.e.*, **2a**, is first validated via quantitative NMR measurements in which **2a**-saturated PNCs were centrifuged, isolated, and redissolved in DMSO-d_6 to break the PNCs into free soluble molecules. An internal reference is added to calculate the binding amount of **2a**, demonstrating ~1% (by weight) of **2a** binding to the PNCs (Figure S20). Such binding experiments imply roughly 130 substrate molecules per PNC (estimated from 10 nm PNC). Surface TEA binding has also been elucidated with IR spectroscopy (Figure 3). To understand the interaction between the substrate and PNCs, **2c** was employed for the IR comparisons. Upon stirring with $CsPbBr_3$ PNCs under dark conditions, the carboxylate stretches of **2c** shifted toward higher wavenumbers (~10 cm^{-1}). Such blue-shifted stretching mode likely results from the positively charged PNC surfaces, suggesting a binding interaction between TEA and the PNC surfaces.

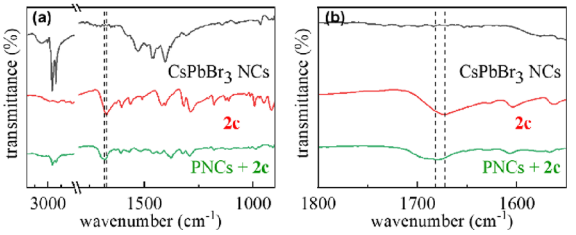

Figure 3. (a) FTIR comparison indicating the surface binding of the substrate via the carboxylate group. (b) Enlarged carboxylate stretches.

2.3. TET-Induced 2 + 2 Cycloaddition Product. To corroborate the quenching studies, a photocatalytic 2 + 2 reaction was set up with TEAs as the reaction substrates and bulk-like PNCs as the catalyst in THF under blue LED illumination (Table 1). Such a neat reaction setup provided a

Table 1. Control Experiment of the PNC TET-Mediated Intermolecular 2 + 2 Cycloaddition

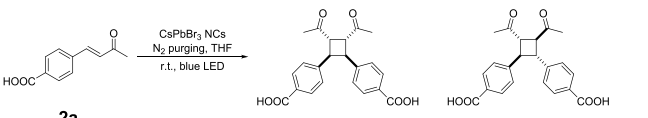

entry	variation from standard conditions[a]	2aa, %[b]	d.r.[b]
1	none	44	>30:1
2	without light	0	N/A
3	without perovskite	0	N/A
4	with a green LED (525 nm)	17	>30:1
5	without N_2 purging	31	>30:1

[a]Conditions: **2a** (0.033 mmol), $CsPbBr_3$ NCs (2 mg), THF (1.2 mL), room temperature, under N_2, blue LED irradiation, 20 h. [b]The yield and diastereomeric ratio were determined by crude ^{1}H NMR using dibromomethane (DBM) as an internal standard.

viable model to directly monitor the reaction progress with ^{1}H NMR. As shown in Figure 4, upon illumination with blue LEDs for 30 min, a readily *E*/*Z* olefin equilibrium of **2a** was observed and, more importantly, an HH-*syn*-addition product **2aa** emerged with characteristic cyclobutane peaks at 4.05 and 4.25 ppm. The rate of formation (Figure S16) suggested that

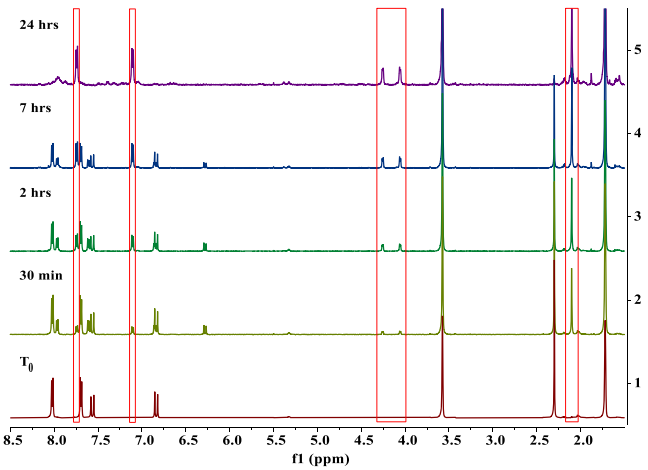

Figure 4. Time-dependent NMR studies of **2a** cycloaddition in THF-d_8 (**2aa** signal circled in red).

https://doi.org/10.1021/acsami.2c03411
ACS Appl. Mater. Interfaces XXXX, XXX, XXX–XXX

2aa is dependent on the concentration of **2a** in a pseudo-second-order relationship. Further illumination leads to the accumulation of **2aa**, and the diminishing of substrate **2a** overall results in a 42% isolated yield.

It is important to point out that neither *anti*-addition 2 + 2 product nor any HT product, as shown in Scheme 1, has been observed on NMR or HPLC scale (Figure S2), rendering a highly diastereomeric selective PNC photocatalysis. The control experiments (Table 1) reveal that light and PNCs are all essential for this reaction. Whereas a molecular photocatalyst, *i.e.*, $Ir(ppy)_3$, leads to a mixture of 2 + 2 products as HH-*anti* (major), HH-*syn* (minor), a trace amount of HT-*syn* and HT-*anti*, a full combination of unbound excited TEAs as expected in Scheme 1. Correspondingly, NMR studies on TEAs with little or no K_{SV} discussed above showed no 2 + 2 product. Substrate **4** or **5**, although showing a significant K_{SV}, renders no product, likely due to a charge transfer quenching process and not TET. The cycloaddition of **2a** under otherwise identical conditions but with irradiation under a green (525 nm) LED also leads to **2aa** (Table 1, entry 4). This implies that bulk PNCs are effective for the TET process observed here, while quantum-confined PNCs, which are not excited by the green LED, are not necessary for the TET process in this reaction. Together, these results demonstrate the following: (1) TEA substrates necessitate a suitable anchoring group; (2) if the excited TEA is in unbound form for 2 + 2 cycloaddition, an *anti*-addition product would otherwise be preferred; (3) bulk-like PNCs are also effective toward 2 + 2 cycloadditions.

We have extended the scope of the photocatalytic 2 + 2 cycloadditions and synthesized respective *syn*-products under *homo*-additions and *hetero*-additions as shown in Table 2 with bulk-like PNCs. In general, *hetero* 2 + 2 additions (*i.e.*, **2ac**, **2bc**, and **2cd**) have been observed with a higher yield than *homo*-additions. Meanwhile, the *homo*-addition demonstrated a polymeric byproduct as evidenced by NMR (Figure S14), perhaps resulting from PNC surface-template polymerization

Table 2. Representative Bulk-like PNC-Induced HH-*syn*-Selective 2 + 2 Cycloadditions[a,b]

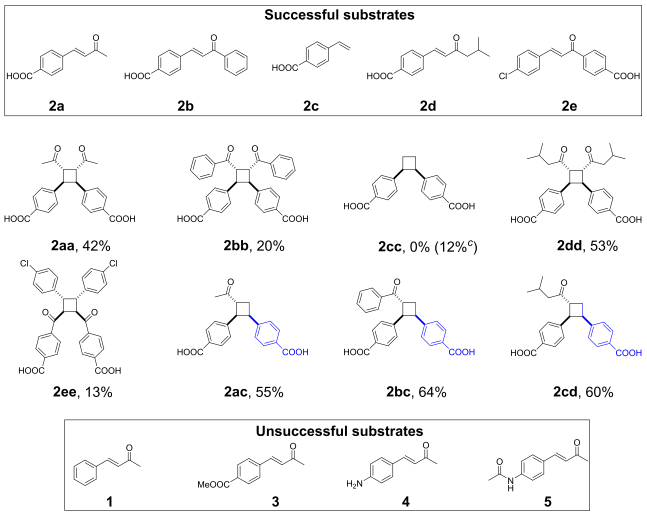

[a]Reactions ran under standard conditions. For *hetero*-coupling, **2c** (0.033 mmol, 3.0 equiv) was used as a coupling partner to react with chalcone derivatives (0.011 mmol, 1.0 equiv). [b]All yields are isolated yields via column chromatography using $AcOH/CH_2Cl_2$ as eluent. [c]Reaction ran for 40 h and oleylamine (5 μL) was used as an additive.

of the excited olefin TEAs. **2c** cannot be excited (E_T = 2.51 eV) under the current conditions, but when added in excess, it can function as a reagent to capture the excited TEAs for the 2 + 2 cycloaddition, diminishing the polymeric byproduct formation route. Note that no **2cc** was produced unless a catalytic amount of oleylamine was added, although the yield is still low. This may result from a previously observed etching effect[46] of PNCs under the presence of both aromatic acids and primary amines. Such an effect results in a blue-shift of the PNC PL (Figure S25) and hence activates substrate **2c** with a higher E_T. We have discussed below the cycloaddition reaction dynamics to illustrate the PNC-induced TET mechanism and also to elaborate the discrepancy among these substrates.

2.4. TET Dynamics. Ultrafast spectroscopy is critical to understand the photocatalytic reaction dynamics. Here, we relied on it to illustrate the TET process within this light-induced cycloaddition pathway. A previous ultrafast study demonstrated that TET to TEAs (*i.e.*, PAHs) was not observed for bulk-like $CsPbBr_3$ PNCs, while the TET efficiency gradually increases when quantum-confined perovskite NCs were employed.[25] A highly size-dependent TET rate was obtained as a function of carrier probability density on the NC surface ($|\Psi s|^2$) for varying NC sizes. The highest TET efficiency was observed for a blue NC (size = 3.5 nm) with the strongest quantum confinement.

The TET dynamics are drastically different under the current 2 + 2 cycloaddition system. TET dynamic exploration has also been compared among a series of TEAs (Figure 5). Typical pseudocolor images corresponding to PNCs, PNCs + **2a** (labeled **2a**), PNCs + **2b** (labeled **2b**), and PNCs + **2c** (labeled **2c**) in THF were generated where the *y*-axis indicates the pump-probe delay time, and the *x*-axis indicates the probe wavelength. The color indicates the intensity of the photo-

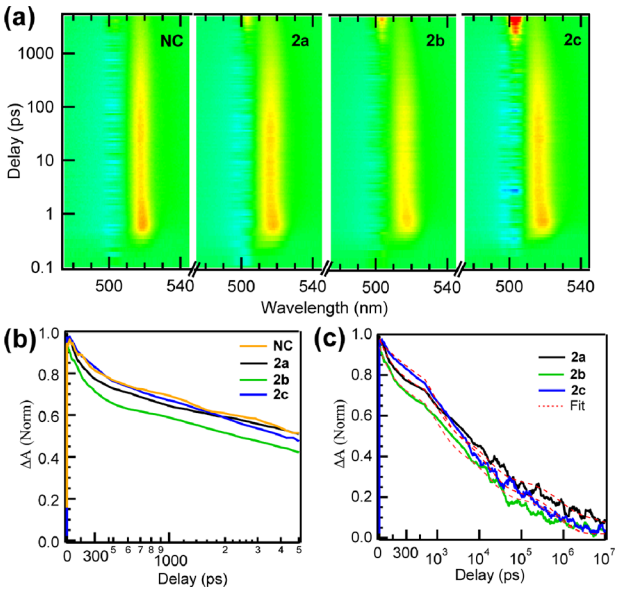

Figure 5. (a) Pseudocolor image plot of the TA experiments of NC, **2a**, **2b**, and **2c** in THF. The *y*-axis indicates pump-probe delay time, and the *x*-axis indicates the probe wavelength. The bright red color corresponds to photoinduced NC exciton ground-state bleach, while blue corresponds to photoinduced absorption. (b) Normalized TA kinetics probed at the center of the NC exciton bleach spectrum for NC, **2a**, **2b**, and **2c**. (c) Normalized TA kinetics and fits for **2a**, **2b**, and **2c**.

https://doi.org/10.1021/acsami.2c03411
ACS Appl. Mater. Interfaces XXXX, XXX, XXX−XXX

induced absorption (PIA) or photo-induced ground-state bleach (GSB). The GSB dynamics can be followed to monitor the reaction progress.[42,47,48] In the pseudocolor image, the bright red color corresponds to the photo-induced GSB of the PNCs. Compared with the isolated PNCs, the dynamics for **2b** exhibit a faster overall decay than that observed for the isolated PNCs, indicating fast TET. The dynamics for **2a**, on the other hand, show an initial faster decay around 107 ps followed by a much slower decay. This could indicate that the energy of the triplet state of **2a** (E_T = 2.36 eV[23]) can transfer back to the NCs since they have similar energies.[26] In the case of **2c**, the kinetics are almost identical to the isolated NCs, suggesting no TET or charge transfer to **2c** (E_T = 2.51 eV). This also corroborates well with the experimental observation that *homo*-cycloaddition of **2c** to **2cc** is not occurring under our current reaction conditions. To further elucidate the TET, we extended the kinetic studies of **2a, 2b**, and **2c** to 10 μs. We first analyze the kinetics for **2c**. Since there is no TET for **2c**, we can use a previously established fitting procedure to model its kinetics.[42] We describe the TA kinetics with three parallel processes in eq 1 (Table S8):

$$[N(t)] = -A_1 \cdot e^{-t/\tau_1} - A_2 \cdot e^{-t/\tau_2} - A_3 \cdot e^{-t/\tau_3} \quad (1)$$

where $N(t)$ is the exciton population at a pump-probe delay of t, and τ_1, τ_2, and τ_3 are the three processes that describe charge recombination of the NCs.[49] For **2c**, the best-fit time constants are 922 ± 47 ps, 16.6 ± 1.0 ns, and 840 ± 49 ns, which correspond to surface trapping (922 ps) and radiative recombination (16.6 and 840 ns, possibly due to electrons and holes, Table S8), respectively.[50] When TET occurs, we introduce a term to describe the fraction of nanocrystals (f_2) that undergo TET and subsequent recombination. Due to the heterogeneous nature of the reaction, a portion of NCs might not have a TEA nearby and, therefore, this fraction (f_1) remains unchanged.[42] Thus, eq 1 can be rewritten as follows:

$$[N(t)] = f_1(-A_1 \cdot e^{-t/\tau_1} - A_2 \cdot e^{-t/\tau_2} - A_3 \cdot e^{-t/\tau_3}) + f_2(-B_1 \cdot e^{-t/\tau_4} - B_2 \cdot e^{-t/\tau_5}) \quad (2)$$

Here, τ_4 is the energy transfer time and τ_5 is the recombination lifetime. Note here that when TET occurs to induce 2 + 2 cycloaddition reactions, there will be no recombination afterward and the whole process is dominated by τ_4. In colloidal systems, characteristic charge/energy transfer times from nanocrystals to molecules can span from a few ps to a few ns.[51−53] Here, the fitting results are shown in Figure 5c and the best-fit parameters are listed in Table 3, rendering ∼110 ps fast TET from bulk PNCs to TEAs under the current reaction pathway and a moderate fraction of *ca.* 13−20% bulk-like PNCs undergoing the TET process to the TEAs.

A previous ultrafast study demonstrated that the TET efficiency to TEAs was gradually increased when a quantum-confined perovskite NC was employed.[25] For bulk-like $CsPbBr_3$ nanocrystals, the TET efficiency is very low (0.006), which is quite different from our 2 + 2 cycloaddition system studied here. A fast TET rate on the order of ∼110 ps is illustrated by transient absorption spectroscopy in our system. Such a trend might be related to a surface state-mediated energy transfer process, which has been observed for PbS quantum dots[54,55] and bulk metal halide perovskite systems.[41] With surface state mediation, triplet states could efficiently transfer to the TEAs and result in a 2 + 2 cycloaddition reaction.

Table 3. TET Fit Parameters

reactant	τ_4 (ps)	f_2
2a	109 ± 18	20 ± 5%
2b	107 ± 19	13 ± 3%
2c	no TET	N/A

2.5. DFT Studies to Illustrate High Diastereomeric Selectivity. We have employed DFT calculations to illustrate the surface binding thermodynamics that are responsible for the highly *syn*-selective 2 + 2 product. DFT calculations have been applied to estimate the binding energy in Scheme 2,

Scheme 2. Proposed Reaction Paths

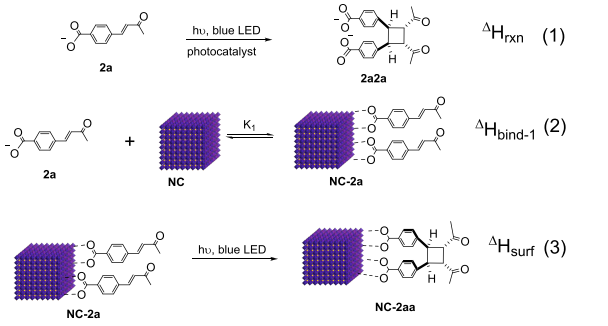

employing the same methodology as reported lately on a CdSe quantum dot system.[56] A 4 × 4 cubic matrix from a perovskite crystal structure (Pb−Br, 2.97 Å; Cs−Cs, 5.94 Å[57]) with a Cs-rich surface is used without optimization as shown in Figure 6. The binding energies were computed with DFT using a B3LYP functional and Ahlrichs double-ζ basis set with a polarization function, Def2-SVP, with the dispersion terms including D3BJ (Grimme's third-generation dispersion and Becke−Johnson damping) (more details shown in the Supporting Information, Section 14) We employed **2a** as an example to illustrate the high diastereomeric selectivity in this reaction pathway as proposed in Scheme 2. We found that reaction (1) is exothermic, $^{\Delta}H_{rxn} \approx -6$ kcal/mol in *syn*-mode, while $^{\Delta}H_{rxn} \approx -11$ kcal/mol in *anti*-addition in THF. Without surface binding, *i.e.*, under unbound TET from a molecular photocatalyst, an *anti*-addition 2 + 2 product will be preferred. This corroborates with previous reports that reaction (1) with homogeneous Ir- or Ru-based molecular sensitizer, *anti*-2 + 2 cyclobutanes were dominant.[16−21]

With PNC surface binding, a clear discrepancy of reaction paths is shown in Scheme 2. Previous experimental evidence[58] and theoretical explorations[59] both suggested that $CsPbBr_3$ PNCs present an excess Cs^+ with a positively charged surface. We adopted a positively charged Cs-rich PNC surface, which prefers binding to the carboxylate substrates as shown in Figure 6a,b accordingly.[59] Three carboxylate-binding modes, **2a**-chelating to one Cs ion, **2a**-bridging to two adjacent Cs ions, and **2a**-bridging to two diagonal Cs ions, have all been compared (Figure S27). The binding energy comparison indicated that **2a**-bridging (shown in Figure 6c) demonstrated the most stable binding enthalpy and therefore was selected for further binding exploration modes. Respective binding intermediates in reactions (2) and (3), Scheme 2, were optimized as shown in Figure 6b, and their energy comparisons are illustrated in Figure 6c. The key intermediate **NC-2a**

https://doi.org/10.1021/acsami.2c03411
ACS Appl. Mater. Interfaces XXXX, XXX, XXX−XXX

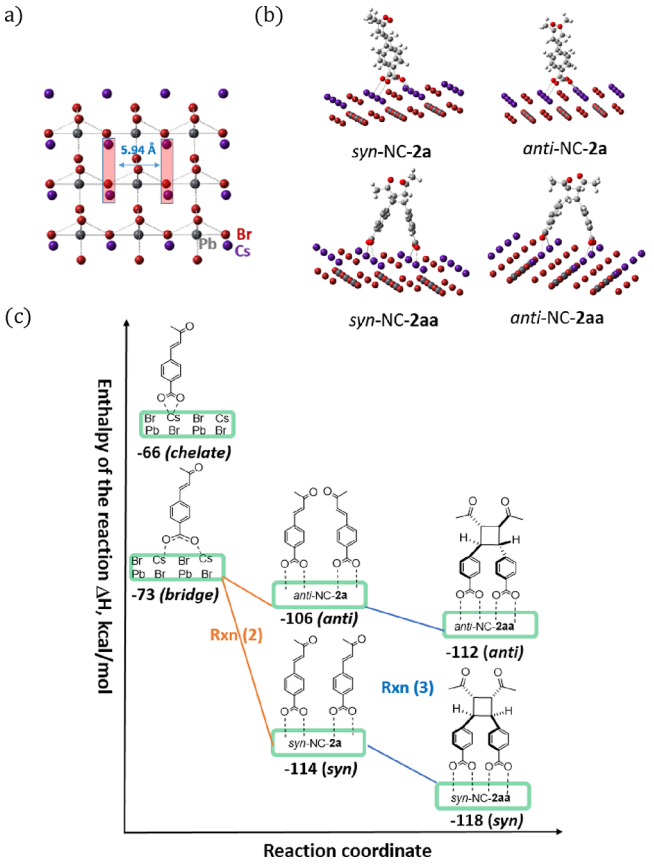

Figure 6. (a) Perovskite $CsPbBr_3$ surface (frozen structure from the crystal structure); (b) optimized binding structures of **2a** and **2aa** via *syn*- and *anti*-modes on NC; (c) binding enthalpy of the reaction path.

demonstrated a stark discrepancy with reaction (1) in which *syn*-**NC-2a** demonstrates ∼−8 kcal/mol change of enthalpy more stable than *anti*-**NC-2a**. The **NC-2aa** intermediate also demonstrated a similar energy discrepancy, −6 kcal/mol with preference to *syn*-**NC-2aa**. A similar energy discrepancy on a CdSe quantum dot surface where *ca.* −17 kcal/mol energy stabilization was noted for the *syn*-intermediate over *anti*-intermediate.[56] In general, these DFT results corroborate well with our experimental observation where the *syn*-product is dominant in this TET-based PNC photocatalysis.

The two **2a** ligands, *syn*- or *anti*-binding on the PNC surface, after TET-induced 2 + 2 cycloaddition, determined the final *syn*- or *anti*-**2aa** product, respectively. The $^{\Delta}H_{rxn}$ of overall reaction (1) does not necessarily govern the final diastereomeric selectivity under the template reaction path. Rather, both binding intermediates show a lower energy path in *syn*-mode than the respective *anti*-mode. We may rationalize that the π-orbital overlap between **2a** substrates in *syn*-mode delocalized extensively from the phenyl group to conjugate motifs, *i.e.*, C═C and C═O bonds; however, such an overlap is significantly diminished in *anti*-mode, with only a phenyl-based π-overlap but excluding effective π-interaction in the C═C—C═O area. Such π-orbital overlap extension here might play a more significant role on a flat cubic surface of the perovskite NCs. Therefore, *syn*-binding **NC-2a** is preferred with *ca.* −8 kcal/mol energy stabilization. Such an energy term might be the key energy component for our observation here in this highly diastereomeric *syn*-selective cycloaddition.

3. CONCLUSIONS

In conclusion, triplet excitons that are generally confined within semiconductors have been successfully transferred from PNCs to organic olefin substrates and induce highly selective photocatalytic 2 + 2 cycloadditions. We found that under our designed reaction pathway, the quantum confinement is not necessary to entail the TET event, perhaps indicating a discrepant TET mechanism from perovskite to PAHs. Bulk PNCs with uncontrolled size (>10 nm) are significantly more accessible for catalyst production and, hence, a reliable and economical photocatalyst for this type of *syn*-selective reaction. The TET-induced reaction dynamics have been illustrated with ultrafast spectroscopy. Fast dynamics (∼110 ps) and a moderate fraction (∼20%) of TET were observed from bulk PNCs to the respective TEAs. A DFT theoretical method that has been previously employed on the CdSe QD system is successfully explored here to elucidate the high selectivity in this PNC surface-template 2 + 2 reaction path. A nontrivial amount of binding enthalpy, up to −8 kcal/mol, likely accounting from the extended π-orbital overlap under *syn*-mode, is found to stabilize the key *syn*-addition intermediate. Our exploration here may reveal a new triplet energy conversion pathway to employ bulk semiconductors for photocatalytic organic synthesis.

4. EXPERIMENTAL SECTION

4.1. Materials. Commercially available reagents were purchased form Sigma-Aldrich (US) or TCI Chemicals (US). Anhydrous, unstable tetrahydrofuran (THF) was purchased from Alfa Aesar and was directly used under N_2 protection for the photochemical reaction setup. All other solvents were purchased from Alfa Aesar or Fisher Scientific and used as received. Household blue LED light bulbs (14 W) were purchased from Amazon and were used for all photochemical reactions, unless otherwise noted. Silica gels (P60, 40−63 μm, 60 Å) used for column chromatography were purchased from SILICYCLE (Canada).

4.2. Preparation of the $CsPbBr_3$ Photocatalyst. $CsPbBr_3$ NCs were synthesized by minor modification of the literature method.[60] The Cs-oleate precursor solution was prepared by loading Cs_2CO_3 (0.204 g), oleic acid (OA, 625 μL), 1-octadecene (1-ODE, 10 mL) in a 50 mL two-necked round-bottom flask equipped with a suitable stirring bar. The resulting dispersion was subject to vacuum drying for 1 h at 120 °C and then charged with N_2 and heated to 150 °C until all Cs_2CO_3 reacted with OA. The Cs-oleate precursor solution was kept at 120 °C for the next-step use. Meanwhile, 1-ODE (5 mL) and $PbBr_2$ (0.069 g, 0.188 mmol) were loaded into a 25 mL Schlenk tube equipped with a suitable stirring bar, dried under vacuum for 1 h at 120 °C, and then charged with N_2 followed by the addition of dried oleylamine (OlAm, 0.5 mL) and dried OA (0.5 mL). After complete solubilization of $PbBr_2$, the temperature of the resulting solution was raised to and kept at 170 °C. The prepared Cs-oleate solution (0.4 mL, 0.125 M in 1-ODE) was quickly injected by using a 1 mL syringe, and 5 s later, the reaction mixture was taken out from the hot plate and cooled by immersion in an ice-water bath for 1 min. To the resulting yellow-greenish mixture was added the same volume of methyl acetate (MeOAc, ∼6.5 mL), and $CsPbBr_3$ NCs were collected by centrifugation at 4k rpm for 30 min and further washed with MeOAc (∼3 mL). The residual solvent was removed by a house vacuum for 2 h.

4.3. Photocatalytic 2 + 2 Cycloaddition Reaction. A 4 mL vial was charged with a 4-vinylbenzoic acid derivative (0.011 mmol, 1.0 equiv) and a coupling partner of 4-vinylbenzoic acid (**2c**, 0.033 mmol, 3.0 equiv) with $CsPbBr_3$ NCs (2 mg) and a suitable-sized magnetic stirring bar. N_2-protected preservative-free THF (1.2 mL) was used as the solvent. While stirring slowly, the reaction solution was purged with 99.998% N_2 for 20 min through a cap with Teflon septa and

https://doi.org/10.1021/acsami.2c03411
ACS Appl. Mater. Interfaces XXXX, XXX, XXX−XXX

sealed with parafilm. The reaction vial was then placed in the middle of but ~5 cm away from two face-to-face (~10 cm) 14 W household blue LED bulbs and stirred at 1200 rpm without heating for 20 h.

4.4. Characterization. The ^{1}H NMR and ^{13}C NMR spectra were acquired using a Varian VNMRS 400 spectrometer or Varian Inova 500 spectrometer The steady-state emission spectra were acquired using a HORIBA Fluoromax-3 spectrofluorometer. Powder XRD data was taken on an X-ray Powder Diffraction Philips Empyrean using a piece of glass slide as a sample holder. The UV−Vis absorption spectra were acquired using a Thermo Scientific GENESYS 30 Visible Spectrophotometer. The IR spectra were measured on a Thermo Fisher Scientific Nicolet iS50 FTIR Spectrometer. TEM images were collected on a FEI Tecnai 12 transmission electron microscope.

4.5. TA Experiment Setup. Transient absorption measurement was carried out on a Ti:sapphire laser amplifier (Coherent Libra; 800 nm; pulse duration, ~200 fs; ~4 mJ/pulse and 1 kHz repetition rate) and pump-probe transient absorption spectrometer (Helios, Ultrafast System). The fundamental beam (800 nm) was split in two beams. One beam was sent to an optical parametric amplifier to generate the pump pulse at 500 nm (2.48 eV), and its intensity was attenuated by two neutral density filter wheels. The other 800 nm beam was focused into a sapphire to generate a white light probe (450−780 nm). The probe delay can be up to ~5 ns, which is tuned by a delay line. For the time delay longer than 5 ns, a fiber laser was used to generate the white light probe pulse and the delay was controlled electronically (EOS, Ultrafast Systems). The pump and probe were focused and overlapped onto the sample. The probe size is ~200 μm, and pump beam size is ~500 μm. The beam size is defined as the radius of an aperture that contains ($1/e^2$) of the total power. The samples are constantly stirred to give reactants enough time to diffuse.

4.6. DFT Calculation. All DFT calculations were carried out with Gaussian 16. The geometries were visualized with GaussView 6. The DFT methodology was employed following a previous report on a CdSe quantum dot system.[56] A 4 × 4 cubic matrix from a perovskite crystal structure (Pb−Br, 2.97 Å; Cs−Cs, 5.94 Å[57]) with a Cs-rich surface was used without optimization. The binding energies were computed with DFT using the B3LYP functional and Ahlrichs double-ζ basis set with a polarization function, Def2-SVP, with the dispersion terms including D3BJ (Grimme's third-generation dispersion and Becke−Johnson damping).

■ ASSOCIATED CONTENT

Supporting Information

The Supporting Information is available free of charge at https://pubs.acs.org/doi/10.1021/acsami.2c03411.

Additional experimental details for preparation of perovskite catalysts and photocatalytic cycloaddition setup, NMR spectra for all compounds, DFT calculations, UV−Vis and PL spectra, TEM measurements, ultrafast transient absorption study, and references (PDF)

■ AUTHOR INFORMATION

Corresponding Author

Yong Yan − *Department of Chemistry and Biochemistry, San Diego State University, San Diego, California 92182, United States;* orcid.org/0000-0001-6361-0541; Email: yong.yan@sdsu.edu

Authors

Yixiong Lin − *Department of Chemistry and Biochemistry, San Diego State University, San Diego, California 92182, United States;* orcid.org/0000-0001-5769-5315

Mariana Avvacumova − *Department of Chemistry and Biochemistry, San Diego State University, San Diego, California 92182, United States*

Ruilin Zhao − *Department of Chemistry and Biochemistry, San Diego State University, San Diego, California 92182, United States*

Xihan Chen − *National Renewable Energy Laboratory, Golden, Colorado 80401, United States*

Matthew C. Beard − *National Renewable Energy Laboratory, Golden, Colorado 80401, United States;* orcid.org/0000-0002-2711-1355

Complete contact information is available at: https://pubs.acs.org/10.1021/acsami.2c03411

Notes

The authors declare no competing financial interest.

■ ACKNOWLEDGMENTS

The photocatalytic organic C−C bond formation reaction exploration is supported by NSF award 1851747 to Y.Y. The energy transfer mechanism study on hybrid materials is supported by the Center for Hybrid Organic Inorganic Semiconductors for Energy (CHOISE), an Energy Frontier Research Center funded by the Office of Science, Office of Basic Energy Sciences, within the US Department of Energy. Part of this work was authored by the Alliance for Sustainable Energy, LLC, and the manager and operator of the National Renewable Energy Laboratory for DOE under contract no. DE-AC36-08GO28308. The views expressed in the article do not necessarily represent the views of the DOE or the U.S. Government. The calculations were performed using computational resources sponsored by the Department of Energy's Office of Energy Efficiency and Renewable Energy and located at the National Renewable Energy Laboratory.

■ REFERENCES

(1) Dey, A.; Ye, J.; De, A.; Debroye, E.; Ha, S. K.; Bladt, E.; Kshirsagar, A. S.; Wang, Z.; Yin, J.; Wang, Y.; Quan, L. N.; Yan, F.; Gao, M.; Li, X.; Shamsi, J.; Debnath, T.; Cao, M.; Scheel, M. A.; Kumar, S.; Steele, J. A.; Gerhard, M.; Chouhan, L.; Xu, K.; Wu, X.-G.; Li, Y.; Zhang, Y.; Dutta, A.; Han, C.; Vincon, I.; Rogach, A. L.; Nag, A.; Samanta, A.; Korgel, B. A.; Shih, C.-J.; Gamelin, D. R.; Son, D. H.; Zeng, H.; Zhong, H.; Sun, H.; Demir, H. V.; Scheblykin, I. G.; Mora-Seró, I.; Stolarczyk, J. K.; Zhang, J. Z.; Feldmann, J.; Hofkens, J.; Luther, J. M.; Pérez-Prieto, J.; Li, L.; Manna, L.; Bodnarchuk, M. I.; Kovalenko, M. V.; Roeffaers, M. B. J.; Pradhan, N.; Mohammed, O. F.; Bakr, O. M.; Yang, P.; Müller-Buschbaum, P.; Kamat, P. V.; Bao, Q.; Zhang, Q.; Krahne, R.; Galian, R. E.; Stranks, S. D.; Bals, S.; Biju, V.; Tisdale, W. A.; Yan, Y.; Hoye, R. L. Z.; Polavarapu, L. State of the Art and Prospects for Halide Perovskite Nanocrystals. *ACS Nano* **2021**, *15*, 10775−10981.

(2) Yang, Y.; Yang, M.; Moore, D. T.; Yan, Y.; Miller, E. M.; Zhu, K.; Beard, M. C. Top and Bottom Surfaces Limit Carrier Lifetime in Lead Iodide Perovskite Films. *Nat. Energy* **2017**, *2*, 16207.

(3) Yang, Y.; Ostrowski, D. P.; France, R. M.; Zhu, K.; van de Lagemaat, J.; Luther, J. M.; Beard, M. C. Observation of a Hot-Phonon Bottleneck in Lead-Iodide Perovskites. *Nat. Photonics* **2016**, *10*, 53−59.

(4) Yang, Y.; Yang, M.; Li, Z.; Crisp, R.; Zhu, K.; Beard, M. C. Comparison of Recombination Dynamics in $CH_3NH_3PbBr_3$ and $CH_3NH_3PbI_3$ Perovskite Films: Influence of Exciton Binding Energy. *J. Phys. Chem. Lett.* **2015**, *6*, 4688−4692.

(5) Xing, G.; Mathews, N.; Sun, S.; Lim, S. S.; Lam, Y. M.; Grätzel, M.; Mhaisalkar, S.; Sum, T. C. Long-Range Balanced Electron- and Hole-Transport Lengths in Organic-Inorganic $CH_3NH_3PbI_3$. *Science* **2013**, *342*, 344−347.

(6) Dong, Q.; Fang, Y.; Shao, Y.; Mulligan, P.; Qiu, J.; Cao, L.; Huang, J. Electron-Hole Diffusion Lengths > 175 μm in Solution-Grown $CH_3NH_3PbI_3$ Single Crystals. *Science* **2015**, *347*, 967−970.
(7) Zhu, X.; Lin, Y.; Sun, Y.; Beard, M. C.; Yan, Y. Lead-Halide Perovskites for Photocatalytic α-Alkylation of Aldehydes. *J. Am. Chem. Soc.* **2019**, *141*, 733−738.
(8) Zhu, X.; Lin, Y.; San Martin, J.; Sun, Y.; Zhu, D.; Yan, Y. Lead Halide Perovskites for Photocatalytic Organic Synthesis. *Nat. Commun.* **2019**, *10*, 2843.
(9) Martin, J. S.; Zeng, X.; Chen, X.; Miller, C.; Han, C.; Lin, Y.; Yamamoto, N.; Wang, X.; Yazdi, S.; Yan, Y.; Beard, M. C.; Yan, Y. A Nanocrystal Catalyst Incorporating a Surface Bound Transition Metal to Induce Photocatalytic Sequential Electron Transfer Events. *J. Am. Chem. Soc.* **2021**, *143*, 11361−11369.
(10) Wu, W.-B.; Wong, Y.-C.; Tan, Z.-K.; Wu, J. Photo-Induced Thiol Coupling and C−H Activation Using Nanocrystalline Lead-Halide Perovskite Catalysts. *Catal. Sci. Technol.* **2018**, *8*, 4257−4263.
(11) Hong, Z.; Chong, W. K.; Ng, A. Y. R.; Li, M.; Ganguly, R.; Sum, T. C.; Soo, H. S. Hydrophobic Metal Halide Perovskites for Visible-Light Photoredox C−C Bond Cleavage and Dehydrogenation Catalysis. *Angew. Chem., Int. Ed.* **2019**, *58*, 3456−3460.
(12) Dai, Y.; Tüysüz, H. Lead-Free $Cs_3Bi_2Br_9$ Perovskite as Photocatalyst for Ring-Opening Reactions of Epoxides. *ChemSusChem* **2019**, *12*, 2587−2592.
(13) Chen, K.; Deng, X.; Dodekatos, G.; Tüysüz, H. Photocatalytic Polymerization of 3,4-Ethylenedioxythiophene over Cesium Lead Iodide Perovskite Quantum Dots. *J. Am. Chem. Soc.* **2017**, *139*, 12267−12273.
(14) Zhang, M.; Li, Z.; Xin, X.; Zhang, J.; Feng, Y.; Lv, H. Selective Valorization of 5-Hydroxymethylfurfural to 2,5-Diformylfuran Using Atmospheric O_2 and $MAPbBr_3$ Perovskite under Visible Light. *ACS Catal.* **2020**, *10*, 14793−14800.
(15) Zhou, Y.; Yang, M.; Wu, W.; Vasiliev, A. L.; Zhu, K.; Padture, N. P. Room-Temperature Crystallization of Hybrid-Perovskite Thin Films via Solvent-Solvent Extraction for High-Performance Solar Cells. *J. Mater. Chem. A* **2015**, *3*, 8178−8184.
(16) Lei, T.; Zhou, C.; Huang, M.-Y.; Zhao, L.-M.; Yang, B.; Ye, C.; Xiao, H.; Meng, Q.-Y.; Ramamurthy, V.; Tung, C.-H.; Wu, L.-Z. General and Efficient Intermolecular [2+2] Photodimerization of Chalcones and Cinnamic Acid Derivatives in Solution through Visible-Light Catalysis. *Angew. Chem., Int. Ed.* **2017**, *56*, 15407−15410.
(17) Blum, T. R.; Miller, Z. D.; Bates, D. M.; Guzei, I. A.; Yoon, T. P. Enantioselective Photochemistry through Lewis Acid−Catalyzed Triplet Energy Transfer. *Science* **2016**, *354*, 1391−1395.
(18) Daub, M. E.; Jung, H.; Lee, B. J.; Won, J.; Baik, M.-H.; Yoon, T. P. Enantioselective [2+2] Cycloadditions of Cinnamate Esters: Generalizing Lewis Acid Catalysis of Triplet Energy Transfer. *J. Am. Chem. Soc.* **2019**, *141*, 9543−9547.
(19) Zheng, J.; Swords, W. B.; Jung, H.; Skubi, K. L.; Kidd, J. B.; Meyer, G. J.; Baik, M.-H.; Yoon, T. P. Enantioselective Intermolecular Excited-State Photoreactions Using a Chiral Ir Triplet Sensitizer: Separating Association from Energy Transfer in Asymmetric Photocatalysis. *J. Am. Chem. Soc.* **2019**, *141*, 13625−13634.
(20) Strieth-Kalthoff, F.; James, M. J.; Teders, M.; Pitzer, L.; Glorius, F. Energy Transfer Catalysis Mediated by Visible Light: Principles, Applications, Directions. *Chem. Soc. Rev.* **2018**, *47*, 7190−7202.
(21) Strieth-Kalthoff, F.; Glorius, F. Triplet Energy Transfer Photocatalysis: Unlocking the Next Level. *Chem* **2020**, *6*, 1888−1903.
(22) Mongin, C.; Garakyaraghi, S.; Razgoniaeva, N.; Zamkov, M.; Castellano, F. N. Direct Observation of Triplet Energy Transfer from Semiconductor Nanocrystals. *Science* **2016**, *351*, 369−372.
(23) Jiang, Y.; Wang, C.; Rogers, C. R.; Kodaimati, M. S.; Weiss, E. A. Regio- and Diastereoselective Intermolecular [2+2] Cycloadditions Photocatalysed by Quantum Dots. *Nat. Chem.* **2019**, *11*, 1034−1040.
(24) Jiang, Y.; Yang, M.; Wu, Y.; López-Arteaga, R.; Rogers, C. R.; Weiss, E. A. Chemo- and Stereoselective Intermolecular [2 + 2] Photocycloaddition of Conjugated Dienes Using Colloidal Nanocrystal Photocatalysts. *Chem Catal.* **2021**, *1*, 106−116.
(25) Luo, X.; Lai, R.; Li, Y.; Han, Y.; Liang, G.; Liu, X.; Ding, T.; Wang, J.; Wu, K. Triplet Energy Transfer from $CsPbBr_3$ Nanocrystals Enabled by Quantum Confinement. *J. Am. Chem. Soc.* **2019**, *141*, 4186−4190.
(26) Luo, X.; Han, Y.; Chen, Z.; Li, Y.; Liang, G.; Liu, X.; Ding, T.; Nie, C.; Wang, M.; Castellano, F. N.; Wu, K. Mechanisms of Triplet Energy Transfer Across the Inorganic Nanocrystal/Organic Molecule Interface. *Nat. Commun.* **2020**, *11*, 28.
(27) Luo, X.; Liang, G.; Han, Y.; Li, Y.; Ding, T.; He, S.; Liu, X.; Wu, K. Triplet Energy Transfer from Perovskite Nanocrystals Mediated by Electron Transfer. *J. Am. Chem. Soc.* **2020**, *142*, 11270−11278.
(28) DuBose, J. T.; Kamat, P. V. Directing Energy Transfer in Halide Perovskite−Chromophore Hybrid Assemblies. *J. Am. Chem. Soc.* **2021**, *143*, 19214−19223.
(29) Mase, K.; Okumura, K.; Yanai, N.; Kimizuka, N. Triplet sensitization by perovskite nanocrystals for photon upconversion. *Chem. Commun.* **2017**, *53*, 8261−8264.
(30) Jiang, Y.; Weiss, E. A. Colloidal Quantum Dots as Photocatalysts for Triplet Excited State Reactions of Organic Molecules. *J. Am. Chem. Soc.* **2020**, *142*, 15219−15229.
(31) Ravi, V. K.; Markad, G. B.; Nag, A. Band Edge Energies and Excitonic Transition Probabilities of Colloidal $CsPbX_3$ (X = Cl, Br, I) Perovskite Nanocrystals. *ACS Energy Lett.* **2016**, *1*, 665−671.
(32) Lu, Z.; Yoon, T. P. Visible Light Photocatalysis of [2+2] Styrene Cycloadditions by Energy Transfer. *Angew. Chem., Int. Ed.* **2012**, *51*, 10329−10332.
(33) Alonso, R.; Bach, T. A Chiral Thioxanthone as an Organocatalyst for Enantioselective [2+2] Photocycloaddition Reactions Induced by Visible Light. *Angew. Chem., Int. Ed.* **2014**, *53*, 4368−4371.
(34) Zhao, J.; Brosmer, J. L.; Tang, Q.; Yang, Z.; Houk, K. N.; Diaconescu, P. L.; Kwon, O. Intramolecular Crossed [2+2] Photocycloaddition through Visible Light-Induced Energy Transfer. *J. Am. Chem. Soc.* **2017**, *139*, 9807−9810.
(35) Münster, N.; Parker, N. A.; van Dijk, L.; Paton, R. S.; Smith, M. D. Visible Light Photocatalysis of 6π Heterocyclization. *Angew. Chem., Int. Ed.* **2017**, *56*, 9468−9472.
(36) Yuan, Y.; Zhu, H.; Hills-Kimball, K.; Cai, T.; Shi, W.; Wei, Z.; Yang, H.; Candler, Y.; Wang, P.; He, J.; Chen, O. Stereoselective C−C Oxidative Coupling Reactions Photocatalyzed by Zwitterionic Ligand Capped $CsPbBr_3$ Perovskite Quantum Dots. *Angew. Chem., Int. Ed.* **2020**, *59*, 22563−22569.
(37) Du, Y.; Zhang, Y.; Wang, S.; Zhao, K. Highly Stereoselective Dimerization of 3-Alkoxyimino-2-aryl-alkylnitriles via Oxidative Carbon-Carbon. *Synlett* **2009**, *2009*, 1835−1841.
(38) Garakyaraghi, S.; Castellano, F. N. Nanocrystals for Triplet Sensitization: Molecular Behavior from Quantum-Confined Materials. *Inorg. Chem.* **2018**, *57*, 2351−2359.
(39) Wang, H.; Liu, W.; He, X.; Zhang, P.; Zhang, X.; Xie, Y. An Excitonic Perspective on Low-Dimensional Semiconductors for Photocatalysis. *J. Am. Chem. Soc.* **2020**, *142*, 14007−14022.
(40) Moroz, P.; Royo Romero, L.; Zamkov, M. Colloidal Semiconductor Nanocrystals in Energy Transfer Reactions. *Chem. Commun.* **2019**, *55*, 3033−3048.
(41) Wang, L.; Yoo, J. J.; Lin, T.-A.; Perkinson, C. F.; Lu, Y.; Baldo, M. A.; Bawendi, M. G. Interfacial Trap-Assisted Triplet Generation in Lead Halide Perovskite Sensitized Solid-State Upconversion. *Adv. Mater.* **2021**, *33*, 2100854.
(42) Wang, K.; Lu, H.; Zhu, X.; Lin, Y.; Beard, M. C.; Yan, Y.; Chen, X. Ultrafast Reaction Mechanisms in Perovskite Based Photocatalytic C-C Coupling. *ACS Energy Lett.* **2020**, *5*, 566−571.
(43) Garakyaraghi, S.; Mongin, C.; Granger, D. B.; Anthony, J. E.; Castellano, F. N. Delayed Molecular Triplet Generation from Energized Lead Sulfide Quantum Dots. *J. Phys. Chem. Lett.* **2017**, *8*, 1458−1463.
(44) Li, X.; Huang, Z.; Zavala, R.; Tang, M. L. Distance-Dependent Triplet Energy Transfer between CdSe Nanocrystals and Surface Bound Anthracene. *J. Phys. Chem. Lett.* **2016**, *7*, 1955−1959.

https://doi.org/10.1021/acsami.2c03411
ACS Appl. Mater. Interfaces XXXX, XXX, XXX−XXX

(45) Huang, Z.; Tang, M. L. Designing Transmitter Ligands That Mediate Energy Transfer between Semiconductor Nanocrystals and Molecules. *J. Am. Chem. Soc.* **2017**, *139*, 9412−9418.
(46) Koscher, B. A.; Nett, Z.; Alivisatos, A. P. The Underlying Chemical Mechanism of Selective Chemical Etching in $CsPbBr_3$ Nanocrystals for Reliably Accessing Near-Unity Emitters. *ACS Nano* **2019**, *13*, 11825−11833.
(47) Chen, X.; Lu, H.; Li, Z.; Zhai, Y.; Ndione, P. F.; Berry, J. J.; Zhu, K.; Yang, Y.; Beard, M. C. Impact of Layer Thickness on the Charge Carrier and Spin Coherence Lifetime in Two-Dimensional Layered Perovskite Single Crystals. *ACS Energy Lett.* **2018**, *3*, 2273−2279.
(48) Chen, X.; Lu, H.; Yang, Y.; Beard, M. C. Excitonic Effects in Methylammonium Lead Halide Perovskites. *J. Phys. Chem. Lett.* **2018**, *9*, 2595−2603.
(49) Koscher, B. A.; Swabeck, J. K.; Bronstein, N. D.; Alivisatos, A. P. Essentially Trap-Free $CsPbBr_3$ Colloidal Nanocrystals by Postsynthetic Thiocyanate Surface Treatment. *J. Am. Chem. Soc.* **2017**, *139*, 6566−6569.
(50) Li, B.; Huang, H.; Zhang, G.; Yang, C.; Guo, W.; Chen, R.; Qin, C.; Gao, Y.; Biju, V. P.; Rogach, A. L.; Xiao, L.; Jia, S. Excitons and Biexciton Dynamics in Single $CsPbBr_3$ Perovskite Quantum Dots. *J. Phys. Chem. Lett.* **2018**, *9*, 6934−6940.
(51) Wu, K.; Liang, G.; Shang, Q.; Ren, Y.; Kong, D.; Lian, T. Ultrafast Interfacial Electron and Hole Transfer from $CsPbBr_3$ Perovskite Quantum Dots. *J. Am. Chem. Soc.* **2015**, *137*, 12792−12795.
(52) Mandal, S.; George, L.; Tkachenko, N. V. Charge Transfer Dynamics in $CsPbBr_3$ Perovskite Quantum Dots−Anthraquinone/Fullerene (C60) Hybrids. *Nanoscale* **2019**, *11*, 862−869.
(53) Kobosko, S. M.; DuBose, J. T.; Kamat, P. V. Perovskite Photocatalysis. Methyl Viologen Induces Unusually Long-Lived Charge Carrier Separation in CsPbBr3 Nanocrystals. *ACS Energy Lett.* **2020**, *5*, 221−223.
(54) Bender, J. A.; Raulerson, E. K.; Li, X.; Goldzak, T.; Xia, P.; Van Voorhis, T.; Tang, M. L.; Roberts, S. T. Surface States Mediate Triplet Energy Transfer in Nanocrystal−Acene Composite Systems. *J. Am. Chem. Soc.* **2018**, *140*, 7543−7553.
(55) Mahboub, M.; Xia, P.; Van Baren, J.; Li, X.; Lui, C. H.; Tang, M. L. Midgap States in PbS Quantum Dots Induced by Cd and Zn Enhance Photon Upconversion. *ACS Energy Lett.* **2018**, *3*, 767−772.
(56) Jones, L. O.; Mosquera, M. A.; Jiang, Y.; Weiss, E. A.; Schatz, G. C.; Ratner, M. A. Thermodynamics and Mechanism of a Photocatalyzed Stereoselective [2 + 2] Cycloaddition on a CdSe Quantum Dot. *J. Am. Chem. Soc.* **2020**, *142*, 15488−15495.
(57) Goesten, M. G.; Hoffmann, R. Mirrors of Bonding in Metal Halide Perovskites. *J. Am. Chem. Soc.* **2018**, *140*, 12996−13010.
(58) Wei, S.; Yang, Y.; Kang, X.; Wang, L.; Huang, L.; Pan, D. Room-Temperature and Gram-Scale Synthesis of $CsPbX_3$ (X = Cl, Br, I) Perovskite Nanocrystals with 50−85% Photoluminescence Quantum Yields. *Chem. Commun.* **2016**, *52*, 7265−7268.
(59) ten Brinck, S.; Infante, I. Surface Termination, Morphology, and Bright Photoluminescence of Cesium Lead Halide Perovskite Nanocrystals. *ACS Energy Lett.* **2016**, *1*, 1266−1272.
(60) Protesescu, L.; Yakunin, S.; Bodnarchuk, M. I.; Krieg, F.; Caputo, R.; Hendon, C. H.; Yang, R. X.; Walsh, A.; Kovalenko, M. V. Nanocrystals of Cesium Lead Halide Perovskites ($CsPbX_3$, X = Cl, Br, and I): Novel Optoelectronic Materials Showing Bright Emission with Wide Color Gamut. *Nano Lett.* **2015**, *15*, 3692−3696.

https://doi.org/10.1021/acsami.2c03411
ACS Appl. Mater. Interfaces XXXX, XXX, XXX−XXX